Optimal stomatal behaviour around the world

Article *in* Nature Climate Change · March 2015

DOI: 10.1038/nclimate2550

54 authors, including:

Yan-Shih Lin
French National Institute for Agricultural Res…
17 PUBLICATIONS **335** CITATIONS
SEE PROFILE

Belinda E Medlyn
Western Sydney University
121 PUBLICATIONS **7,601** CITATIONS
SEE PROFILE

Remko Duursma
Western Sydney University
88 PUBLICATIONS **2,416** CITATIONS
SEE PROFILE

Han Wang
Northwest A & F University
32 PUBLICATIONS **398** CITATIONS
SEE PROFILE

Published in Nature Climate Change 5, 459 – 464 (2015)

Optimal stomatal behaviour around the world: synthesis of a global stomatal conductance database

Yan-Shih Lin[1], Belinda E. Medlyn[1], Remko A. Duursma[2], I. Colin Prentice[1,3], Owen K. Atkin[4], Craig V.M. Barton[2], Jonathan Bennie[5], Alexandre Bosc[6,7], Mark S.J. Broadmeadow[8], Lucas A. Cernusak[9], Paolo De Angelis[10], John E. Drake[2], Derek Eamus[11], David S. Ellsworth[2], Michael Freeman[12], Oula Ghannoum[2], Teresa E. Gimeno[2], Qingmin Han[13], Kouki Hikosaka[14], Lindsay B. Hutley[15], Jeff W. Kelly[1], Kihachiro Kikuzawa[16], Pasi Kolari[17], Kohei Koyama[16,18], Jean-Marc Limousin[19], Maj-Lena Linderson[20], Markus Löw[21], Cate Macinins-Ng[22], Nicolas K. Martin-StPaul[23], Patrick Meir[24], Teis N. Mikkelsen[25], Patrick Mitchell[26], Jesse B. Nippert[27], Yusuke Onoda[28], Maarten Op de Beeck[29], Victor Resco de Dios[30], Ana Rey[31], Alistair Rogers[32], Lucy Rowland[24], Samantha A. Setterfield[15], Wei Sun[33], Lasse Tarvainen[34], Sabine Tausz-Posch[21], David T. Tissue[2], Johan Uddling[35], Göran Wallin[35], Jeff M. Warren[36], Lisa Wingate[6], Joana Zaragoza-Castells[24]

[1]: Department of Biological Sciences, Macquarie University, North Ryde, NSW 2109, Australia

[2]: Hawkesbury Institute for the Environment, University of Western Sydney, Penrith, New South Wales 2751, Australia

[3]: Grantham Institute and Division of Ecology and Evolution, Imperial College, Silwood Park Campus, Ascot SL5 7PY, United Kingdom

[4]: Division of Plant Sciences, Research School of Biology, The Australian National University, Canberra, Australian Capital Territory 0200, Australia

[5]: Environment and Sustainability Institute, University of Exeter, Penryn, United Kingdom

[6]: Institut National de la Recherche Agronomique, Villenave d'Ornon F-33140, France

[7]: Bordeaux Sciences Agro, UMR 1391 ISPA, Gradignan F-33170, France

[8]: Climate Change Forest Services, Forestry Commission England, United Kingdom

[9]: James Cook University, Cairns, Queensland 4879, Australia

[10]: Department for Innovation in Biological, Agro-food and Forest systems, University of Tuscia, Via San Camillo de Lellis, Viterbo 01100, Italy

[11]: School of Life Sciences , University of Technology, Sydney, New South Wales 2007, Australia

[12]: Department of Ecology, Swedish University of Agricultural Sciences, UPPSALA 75007, Sweden

[13]: Hokkaido Research Center, Forestry and Forest Products Research Institute (FFPRI), Toyohira, Sapporo, Hokkaido 062-8516, Japan

[14]: Graduate School of Life Sciences, Tohoku University, Aoba, Sendai 980-8578, Japan

[15]: Research Institute for Environment and Livelihoods, Charles Darwin University, Casuarina, Northern Territory 0810, Australia

[16]: Department of Environmental Science, Faculty of Bioresources and Environmental Sciences, Ishikawa Prefectural University, Ishikawa 921-8836, Japan

[17]: Department of Physics, University of Helsinki, Finland

[18]: Department of Life Science and Agriculture, Obihiro University of Agriculture and Veterinary Medicine, Obihiro, Hokkaido 080-0834, Japan

[19]: Department of Biology, University of New Mexico, Albuquerque, NM 87131-0001, United States

[20]: Department of Physical Geography and Ecosystem Science, Lund University, Sweden

[21]: Department of Agriculture and Food Systems, University of Melbourne, Creswick, Victoria 3363, Australia

[22]: School of Environment, Unversity of Auckland, Auckland 1142, New Zealand

[23]: Université Paris-Sud, Laboratoire Ecologie, Systématique et Evolution, UMR8079, Orsay F-91405, France

[24]: School of Geosciences, The University of Edinburgh, Edinburgh EH8 9XP, United Kingdom

[25]: Center for Ecosystems and Environmental Sustainability, Department of Chemical and Biochemical engineering, Technical University of Denmark, DK-4000 Roskilde, Denmark

[26]: CSIRO Ecosystem Sciences, Sandy Bay, Tasmania 7005, Australia

[27]: Division of Biology, Kansas State University, Manhattan, KS 66505, United States

[28]: Division of Environmental Science and Technology, Graduate School of Agriculture, Kyoto University, Oiwake, Kitashirakawa, Kyoto 606-8502, Japan

[29]: Research Group Plant and Vegetation Ecology, University of Antwerp, Wilrijk 2610, Belgium

[30]: Producció Vegetal i Ciència Forestal, Universitat de Lleida, Lleida 25198, Spain

[31]: Department of Biogeography and Global Change, MNCN-CSIC, Spanish Scientific Council, Madrid 28006, Spain

[32]: Environmental and Climate Sciences Department, Brookhaven National Laboratory, Upton, NY 11973-5000, United States

[33]: Institute of Grassland Science, Northeast Normal University, Key Laboratory of Vegetation Ecology, Changchun, Jilin 130024, China

[34]: Department of Forest Ecology and Management, Swedish University of Agricultural Sciences, Umeå 90183, Sweden

[35]: Department of Biological and Environmental Sciences, University of Gothenburg, Göteborg 40530, Sweden

[36]: Environmental Sciences Division, Oak Ridge National Laboratory, Oak Ridge, TN, USA

Main text

Stomatal conductance is a key land surface attribute as it links plant water-use and carbon uptake. In this study we synthesised a globally distributed database of stomatal conductance data sets obtained in the field for a wide range of plant functional types (PFTs) and biomes. We employed a model of optimal stomatal conductance[1] to assess differences in stomatal behaviour. We estimated the model slope coefficient, g_1, which is directly related to the marginal carbon cost of water-use, for each dataset. We then tested how g_1 varies with climatic factors, including temperature and water availability, and across PFTs. We found that g_1 varied considerably among PFTs, with evergreen savanna trees having the largest g_1 (least conservative water-use), followed by C_3 grasses and crops, angiosperm trees, gymnosperm trees, and C_4 grasses. Amongst angiosperm trees, species with larger wood density had a larger marginal carbon cost of water-use, as predicted by the theory underpinning the optimal stomatal model. There was an interactive effect between temperature and moisture availability (on g_1: for wet environments, g_1 was largest in high temperature environments, indicated by high mean annual growing degree days above 0^oC ($mGDD_0$), but it did not vary with $mGDD_0$ across dry environments. These findings provide a robust theoretical framework for understanding and predicting the behaviour of stomatal conductance across biomes and across PFTs that can be applied to regional, continental and global-scale modelling of productivity and ecohydrological processes in a future changing climate.

Earth System Models (ESMs) integrate biogeochemical and biogeophysical land surface processes with physical climate models and have been widely used to demonstrate the

100 importance of land surface processes in determining climate and to highlight the issue of
101 large uncertainties in quatifying land surface processes[2, 3, 4, 5]. Within the biogeophysical
102 components of land surface processes, stomatal conductance plays a pivotal role because it
103 is a key feedback route for carbon and water exchange between the atmosphere and
104 terrestial vegetation. Stomata are small pores on leaves whose behaviour can be regulated
105 by the plant in response to multiple abiotic and biotic factors. Stomatal conductance (g_s) is
106 a major determinant of both transpiration rates and rates of photosynthetic C uptake. .
107 Therefore, our ability to model the global carbon and water cycles under future changing
108 climate depends on our ability to predict stomatal behaviour globally[1], an ability that to-
109 date has remained particularly intractactable . Although there have been previous synthesis
110 studies on plant stomatal conductance and related traits[6, 7, 8, 9], a global scale database and
111 associated mechanistic globally applicable model of g_s that would allow prediction of
112 stomatal behaviour is lacking.
113
114 For this study, we compiled a unique global database of field measurements of stomatal
115 conductance and photosynthesis suitable for extracting model parameters. We employed a
116 model of optimal stomatal conductance[1] to develop hypotheses for how stomatal behaviour
117 should vary with environmental factors and with plant traits associated with hydraulic
118 function. In the optimal stomatal model, the slope parameter, g_1, is proportional to the
119 marginal carbon cost of water-use[1], meaning that plants with smaller g_1 values are more
120 conservative with their water-use and have higher water-use-efficiency (and *vice versa*).
121 Therefore, we hypothesised that variation in g_1 values among climate zones and PFTs
122 should reflect differences in the cost of water transport. We proposed that:
123 (1) g_1 values among PFTs should vary according to the cost of stemwood construction,
124 such that C3 herbaceous species should have the largest g_1 (i.e. least conservative water-

use), followed by angiosperm trees and gymnosperm trees. Since the optimal stomatal theory predicts that, for the same marginal water cost, g_1 should be lower by approximately one-half [10]. We therefore predicted that C4 plants would have the smallest g_1.

(2) For trees, the cost of water transport should increase with wood density, due to the higher cost of wood construction[11] and the generally smaller hydraulic conductance of sapwoos with large density. Therefore within both angiosperms and gymnosprems, trees with highest wood density should have the smallest g_1.

(3) Moisture stress should increase the cost of water-use to the plant, so plants in dry environments should have a larger marginal cost of water-use and lower g_1.

(4) g_1 values should increase with temperature for two reasons. First, we previously showed that g_1 is approximately proportional to a combination term of the carbon cost of water transport and Γ^* (the CO_2 compensation point in absence of photorespiration)[1]. As Γ^* is exponentially dependent on temperature[1, 12], g_1 should similarly increase with temperature. Second, the viscosity of water decreases with increasing temperature, making it less costly to transport water leading to a increased g_1[13].

To test these hypotheses, we collated a globally distributed database of g_s and photosynthesis of 56 field studies, covering a wide range of biomes from Arctic tundra, boreal and temperate forest to tropical rainforest (Table S1). We estimated the model coefficient, g_1, from observations of leaf-level gas exchange (g_s , ratesd of transpiration and net photosynthesis , see Methods) and environmental drivers. We used mean annual degree days above 0°C ($mGDD_0$) and moisture index (MI) derived from observed long-term meteorological data as proxies to quantify the temperature and water availability that are relevant to plant physiological functions for each site[14]. The growing degree days above 0°C is an index of the energy available for completion of the annual life cycle and

quantifies temperature limitations to carbon assimilation and growth[15, 16]. Our database covered a range of $mGDD_0$ from 2.7 to 29.7 ^oC and a range of MI from 0.17 to 3.26, representing the majority of the climatic space for vegetation covered land surfaces (Fig. 1). We then tested how g_1 varies with MI and $mGDD_0$ across PFTs and biomes?.

We found a clear pattern of g_1 variation among different PFTs with evergreen savanna trees having largest g_1, followed by C_3 grasses and crops, angiosperm trees, gymnosperm trees, and C_4 grasses (Table S2 and Fig. 2). For angiosperm trees, g_1 was negatively correlated with wood density, although we did not find any correlation for gymnosperm species (Fig. 3). g_1 significantly increased with both increasing $mGDD_0$ and MI across the entire data set. However, when evaluated as a bivariate relationship (Fig. 2c-d, and Fig. 4a-b) we observed that there was an interactive effect between temperature and moisture availability on g_1: for wet environments, g_1 was largest at sites with high $mGDD_0$, but it varied with $mGDD_0$ to a much smaller degree across dry environments (Table 1 and Fig. 4).

Our results largely supported our hypotheses for how g_1 should vary among PFTs (hypothesis 1) and biomes. The variation in g_1 among PFTs is a result of trade-offs among plant functions such as growth, defence and reproduction, through different resource allocation patterns that aim to achieve the optimal cost-to-benefit ratios[8, 13] Long life-span PFTs, such as evergreen gymnosperm and angiosperm trees, must invest more in building supporting and defence structures relative to short life-span PFTs, such as grasses, so that they can be sustained over many years of biotic and abiotic stress. Such an investment preference has to come at the cost of reduced growth rates[17, 18], meaning reduced the rates of carbon uptake and water loss cost through opening stomata. Therefore we predicted a more conservative water-use strategy in trees (lower g_1) than in C3 grass (higher g_1), and

this was observed in the database. However, evergreen savanna trees formed an exception with a surprisingly large g_1, relative to expectations based upon trees wood density and biomes MI. This may result from the fact that these species have several unique hydraulic functional traits that may offset the carbon cost of water-use which allow them to have a less conservative water use strategy. These hydraulic functional traits include: deep roots to access groundwater, large sapwood area for water transport, narrow but long conduits to reduce the risk of embolism and reduce the cost of conduit wall construction[19, 20] and dry season declines in LAI to balance increased atmospheric aridity in the dry season . This special case of evergreen savanna trees is worthy of further investigation.

We found a significant relationship between g_1 and wood density among angiosperm trees (Fig. 3; excluding savanna angiosperms) which supported our hypothesis that g_1 is negatively correlated with wood density (hypothesis 2). A larger wood density is advantagous for plants that need to avoid hydraulic failure so that they can sustain more negative sapwood water pressures during drought[18]. However, such an investment is at the expense of a reduced capacity for stem water storage, reduced sapwood conductivity and the carbon cost of building wood with higher density[20, 21, 22], and thus leads to a more conservative water-use-strategy. However, we did not find such a relationship among gymnosperm trees. This lack of correlation may be due to the limited variability in wood density in gymnosperms. There are significant differences in the anatomical structure of sapwood between angiosperms and gymnosperms. The majority of angiosperm trees have evolved to separate the water transport structure (i.e. vessels) from the mechanical support structure, while gymnosperm trees do not have such a functional differentiation, as tracheids are used for both water transport and mechanical support[18, 23]. Therefore, wood density is a good proxy for quantifying the trade-offs between transport and support

200 investments for angiosperm trees but not for gymnosperm trees[23]. The distinct differences
201 in the water-use strategy between angiosperm trees and gymnosperm trees (Fig. 2) is
202 consistent with a recent observation that angiosperms maintain a much smaller hydraulic
203 safety margin than gymnosperms[24], showing that angiosperms allow some loss of
204 hydraulic conductivity – a risky strategy – while gymnosperms minimise lossThis
205 evolutionary development confers an advantage to angiosperm trees by allowing them to
206 use water in a less conservative way, thereby increasing their carbon gain relative to
207 gymnosperm trees.
208
209 Our results only partially supported our hypotheses for how g_1 should vary with moisture
210 stress and temperature (hypotheses 3 and 4 as there was an interactive effect between
211 temperature and moisture stress on g_1. This interactive response between MI and $mGDD_0$
212 demonstrates the complexity of how plants co-ordinate their resource allocation strategies
213 along two axes of climatic gradient (Fig. 4). Temperature affects the cost of water transport
214 in such a way that it should be more costly to transport water in a colder environment than
215 in a warmer one. However, lower temperature also comes with water savings as the
216 evaporative demand and photorespiratory cost are lower. The interactive relationship
217 between MI and $mGDD_0$ suggest that the rate of change in g_1 (i.e. the slope of each
218 exponential curve; Fig. S3) along temperature or water availibility gradient is much higher
219 in the wet and warm environments than in dry and cold environments.
220
221 Our study demonstrated the first mechanistically robust framework that can be applied to
222 various scales for understanding and predicting the behaviour of stomatal conductance
223 across biomes and across PFTs. We analysed a global stomatal behaviour data set along
224 two major climatic axes, providing an analytic framework for understanding how

225 stomatal behaviour adapts to the environment. Our findings will allow the ESM
226 community to move on from using empirical stomatal models (ref ref) with tuned
227 parameters to using a more robust, theory-derived optimal stomatal model with meaningful
228 parameters. In addition, we provide a valuable stomatal behaviour database that can be
229 used to parameterise g_s among PFTs and which can be applied directly within ESMs for
230 modelling productivity and ecohydrological processes in a future changing climate across
231 regional, continental and global scales.
232
233

Methods

Source of data

We synthesised published and unpublished leaf gas exchange data sets for a wide range of PFTs and biomes (Table S1). Our database covers 314 species from 56 experiment sites around the world with 17 sites from Australasia, 15 sites from Europe, 14 sites from North America, six sites from Asia, three sites from South America and one site from Africa. Site latitudes range from 42.9^{o}S to 72.3^{o}N although the majority of the sites are within the temperate zone (n=35; latitude range between 23.5^{o} to 55^{o} and between -23.5^{o} and -55^{o}), followed by tropical zone (n=14; latitude range between -23.5^{o} and 23.5^{o}), boreal zone (n=6; latitude range between 55^{o} and 66.5^{o}) and Arctic zone (n=1; latitude range above 66.5^{o}). We used MI and $mGDD_0$ derived from Climate Research Unit data (CRU TS3.1)[25] from 1991 to 2010 using a modified version of the STASH model[26] at a grid resolution of 0.5^{o}. In this derivation, $mGDD_0$ was calculated as the ratio of the annual sum of temperatures above 0^{o}C (growing degree days) to the length of the period with temperatures above 0^{o}C; MI was calculated as the ratio of mean annual precipitation to the equilibrium evapo-transpiration (E_{eq}). We estimated E_{eq} from temperature and net radiation (calculated from monthly mean percentage of cloud cover) based on the Priestley-Taylor equation[26]. The Sea-WiFS fAPAR (fraction absorbed photosynthetically active radiation) product was used to determine areas with green vegetation cover at a grid resolution of 0.5^{o}. The wood density data were obtained from the Global Wood Density Database[23, 27].

Data analysis

We used data points measured at a photosynthetic photon flux density (PPFD) > 0 µmol m^{-2} s^{-1}, and only data collected from the top third of the canopy (what would happen if you used data for PAR> 250 µmol m^{-2} s^{-1} rather than > 0? . Data points with negative

259 photosynthesis rates were excluded. In all cases, species were grown under ambient
260 environmental conditions and were not subjected to any treatments, such as elevated CO_2,
261 temperature, or drought treatments. We employed an optimal stomatal model[1] as:

$$g_s = g_0 + 1.6 \times (1 + \frac{g_1}{\sqrt{D}}) \frac{A}{C_a}$$

262 where D is vapour pressure deficit, A is net photosynthesis rate, C_a is CO_2 concentrtion at
263 leaf surface, and g_0, g_1 are model coefficients for intercept and slope. We used a non-linear
264 mixed-effect model to estimate the model slope coefficient, g_1, for each group separately
265 for various classification schemes as shown in Fig. 2. In all g_1 estimations, we assumed the
266 intercept coefficient, g_0, to be zero to avoid strong correlation between g_0 and g_1 which
267 would mask any interesting variation in g_1. In this model, individual species were assumed
268 to be the random effect to account for the differences in the g_1 slope among species within
269 the same group. To test how g_1 varies with climatic variables (i.e. MI and $mGDD_0$), we
270 first estimated g_1 for each species using non-linear regression. We then used a linear
271 mixed-effect model to test the relationship between g_1, MI and $mGDD_0$. We fitted the
272 model as:

$$\log(g_1) \sim \mathrm{MI} + \mathrm{mGDD}_0 + \mathrm{MI} \times \mathrm{mGDD}_0$$

273 assuming PFTs as the random effect to account for the differences in intercept among PFTs.
274 To evaluate the goodness of fit for linear mix-effect model, we calculated both the
275 marginal R^2 to quantify the proportion of variance explained by the fixed factors alone and
276 the conditional R^2 to quantify the proportion of variance explained by both the fixed and
277 random factors as described in Nakagawa and Holger Schielzeth (2013)[28]. The relationship
278 between g_1 and wood density were tested with a simple linear regression model. All model
279 estimations and statistical analyses were performed within R 3.1.0[29].

References

1. Medlyn BE*, et al.* Reconciling the optimal and empirical approaches to modelling stomatal conductance. *Global Change Biology* **17**, 2134-2144 (2011).

2. Cox PM, Betts RA, Jones CD, Spall SA, Totterdell IJ. Acceleration of global warming due to carbon-cycle feedbacks in a coupled climate model. *Nature* **408**, 184-187 (2000).

3. Sitch S*, et al.* Evaluation of ecosystem dynamics, plant geography and terrestrial carbon cycling in the LPJ dynamic global vegetation model. *Global Change Biology* **9**, 161-185 (2003).

4. Cao M, Woodward FI. Dynamic responses of terrestrial ecosystem carbon cycling to global climate change. *Nature* **393**, 249-252 (1998).

5. Friedlingstein P*, et al.* Climate-carbon cycle feedback analysis: Results from the C4MIP model intercomparison. *Journal of Climate* **19**, 3337-3353 (2006).

6. Schulze E-D, Kelliher FM, Korner C, Lloyd J, Leuning R. Relationships among maximum stomatal conductance, ecosystem surface conductance, carbon assimilation rate, and plant nitrogen nutrition: a global ecology scaling exercise. *Annual Review of Ecology and Systematics*, 629-660 (1994).

7. Kattge J*, et al.* TRY – a global database of plant traits. *Global Change Biology* **17**, 2905-2935 (2011).

8. Wright IJ, Falster DS, Pickup M, Westoby M. Cross-species patterns in the coordination between leaf and stem traits, and their implications for plant hydraulics. *Physiologia Plantarum* **127**, 445-456 (2006).

9. Lloyd J, Farquhar G. 13C discrimination during CO2 assimilation by the terrestrial biosphere. *Oecologia* **99**, 201-215 (1994).

10. Way DA, Katul GG, Manzoni S, Vico G. Increasing water use efficiency along the C3 to C4 evolutionary pathway: a stomatal optimization perspective. *Journal of Experimental Botany*, (2014).

11. Héroult A, Lin Y-S, Bourne A, Medlyn BE, Ellsworth DS. Optimal stomatal conductance in relation to photosynthesis in climatically contrasting Eucalyptus species under drought. *Plant, Cell & Environment* **36**, 262-274 (2013).

12. Medlyn BE*, et al.* Temperature response of parameters of a biochemically based model of photosynthesis. II. A review of experimental data. *Plant Cell and Environment* **25**, 1167-1179 (2002).

13. Prentice IC, Dong N, Gleason SM, Maire V, Wright IJ. Balancing the costs of carbon gain and water transport: Testing a new theoretical framework for plant functional ecology. *Ecology Letters* **17**, 82-91 (2014).

14. Harrison SP, Prentice IC, Barboni D, Kohfeld KE, Ni J, Sutra JP. Ecophysiological and bioclimatic foundations for a global plant functional classification. *Journal of Vegetation Science* **21**, 300-317 (2010).

15. Woodward FI. *Climate and Plant Distribution* Cambridge University Press (1987).

16. Colin Prentice I, Sykes MT, Cramer W. A simulation model for the transient effects of climate change on forest landscapes. *Ecological Modelling* **65**, 51-70 (1993).

17. Enquist BJ, West GB, Charnov EL, Brown JH. Allometric scaling of production and life-history variation in vascular plants. *Nature* **401**, 907-911 (1999).

18. Hacke UG, Sperry JS, Pockman WT, Davis SD, McCulloh KA. Trends in wood density and structure are linked to prevention of xylem implosion by negative pressure. *Oecologia* **126**, 457-461 (2001).

19. Eamus D, O'Grady AP, Hutley L. Dry season conditions determine wet season water use in the wet–tropical savannas of northern Australia. *Tree Physiology* **20**, 1219-1226 (2000).

20. Sperry JS, Meinzer FC, McCulloh KA. Safety and efficiency conflicts in hydraulic architecture: Scaling from tissues to trees. *Plant, Cell and Environment* **31**, 632-645 (2008).

21. Meinzer FC, James SA, Goldstein G, Woodruff D. Whole-tree water transport scales with sapwood capacitance in tropical forest canopy trees. *Plant, Cell and Environment* **26**, 1147-1155 (2003).

22. Bucci SJ, Goldstein G, Meinzer FC, Scholz FG, Franco AC, Bustamante M. Functional convergence in hydraulic architecture and water relations of tropical savanna trees: From leaf to whole plant. *Tree Physiology* **24**, 891-899 (2004).

23. Chave J, Coomes D, Jansen S, Lewis SL, Swenson NG, Zanne AE. Towards a worldwide wood economics spectrum. *Ecology Letters* **12**, 351-366 (2009).

24. Choat B*, et al.* Global convergence in the vulnerability of forests to drought. *Nature* **491**, 752-755 (2012).

25. Harris I, Jones PD, Osborn TJ, Lister DH. Updated high-resolution grids of monthly climatic observations - the CRU TS3.10 Dataset. *International Journal of Climatology* **34**, 623-642 (2014).

26. Gallego-Sala A*, et al.* Bioclimatic envelope model of climate change impacts on blanket peatland distribution in Great Britain. *Climate Research* **45**, 151-162 (2010).

27. Zanne AE*, et al.* Data from: Towards a worldwide wood economics spectrum. Dryad Data Repository (2009).

28. Nakagawa S, Schielzeth H. A general and simple method for obtaining R2 from generalized linear mixed-effects models. *Methods in Ecology and Evolution* **4**, 133-142 (2013).

29. R Core Team. R: A language and environment for statistical computing. R Foundation for Statistical Computing (2014).

Acknowledgements

This research was supported by the Australian Research Council (ARC MIA Discovery Project 1433500-2012-14). A.R. was financially supported in part by The Next-Generation Ecosystem Experiments (NGEE-Arctic) project that is supported by the Office of Biological and Environmental Research in the Department of Energy, Office of Science, and through the United States Department of Energy contract No. DE-AC02-98CH10886 to Brookhaven National Laboratory. M.O.d.B. acknowledges that the Brassica data were obtained within a research project financed by the Belgian Science Policy (OFFQ, contract number SD/AF/02) and coordinated by Dr Karine Vandermeiren at the Open-Top Chamber research facilities of CODA-CERVA (Tervuren, Belgium).

Author contributions

Competing financial interests

The author declear no competing financial interests.

399 **Table 1: Analysis of Variance table for g_1 as a function of MI and $mGDD_0$.**

400

Model						
Variables	**numDF**	**denDF**	**F-value**		**p-value**	**Marginal R^2**
Intercept	1	97	67.08	<	0.001	0.20
MI	1	97	7.50		0.007	**Conditional R^2**
$mGDD_0$	1	97	11.15		0.001	0.59
MI*$mGDD_0$	1	97	1.34		0.250	

401 **Figure legends**

402 **Figure 1: Climatic space covered by the Stomatal Behaviour Synthesis Database, shown**
403 **as mean annual degree days above 0^{o}C (mGDD$_{0;}$ ^{o}C) and moisure index (MI).** Coloured
404 circles represent climatic space for the database, with different colours indicating different
405 plant functional types. Grey hexagons represent global climatic space for which vegetation is
406 present. The global climatic space data were binned by every 1 ^{o}C for mGDD0 and every 0.25
407 for MI.

408

409 **Figure 2: Mean g_1 values for plant functional types defined by different classification**
410 **schemes.** Each bar represents mean ± SE. Panels (b) (c) and (d) include C_3 species data only.

411

412 **Figure 3: Relationship between g_1 and wood density for angiosperm and gymnosperm**
413 **trees.** Savanna tree species (all angiosperms) are indicated separately. Each data point
414 represents mean ±SE of g_1 for individual species fitted with non-linear regression. A linear
415 regression line was only fitted for angiosperm trees due to limited data for gymnosperm trees.
416 The fitted linear regression relationship between g_1 and wood density for angiosperm trees is:
417 g_1= -4.77*WD+ 6.96 (P = 0.0008, R^2 = 0.23). Wood density data were obtained from Global
418 Wood Density Database[23, 27] and are avaible for 45 species in the Stomatal Behaviour Synthesis
419 Database.

420 **Figure 4**: **Estimated and predicted g_1 as a function of mGDD$_0$ and MI.** Panels (a) (b) show
421 the relationship between estimated g_1 and (a) mean annual degree days above 0 ^{o}C temperature
422 (mGDD$_0$; ^{o}C) and (b) moisture index (MI) at experimental sites among species across different
423 plant functional types (PFTs). Each data point represents mean ± SE of g_1 for individual species

fitted with a non-linear regression. Classification of plant functional types are shown in Figure 2e. Panels (c) and (d) are the predicted g_1 under different ranges of MI and $mGDD_0$ presented as a partial regression plot. Predictions in (c) and (d) are from linear mixed-effects model for $\log(g_1)$ assuming PFTs as a random effect to account for the differeces in intercept among PFTs. Colour lines represent the predicted g_1 based on fitted model coefficients (Table S3). Colour dots represent the partial regression predictions at a given fixed MI or $mGDD_0$ level.

Supplementary Materials

Table S1: List of data source.

Data contributor	Location	Species	Reference
Alexandre Bosc	Le Bray, France	*Pinus pinaster*	Bosc, A. (1999) PhD Thesis.
Alistair Rogers	Barrow, AK, USA	Several Arctic species	Unpublished data.
Ana Rey	Glencorse near Edinburgh, Scotland, UK	*Betula pendula*	Rey & Jarvis (1998) Tree Physiology.
Belinda Medlyn	Tumbarumba flux tower, Snowy Mts, NSW, Australia	*Eucalyptus delegatensis*	Medlyn et al. (2007) Tree Physiology.
Cate Macinnis-Ng	Arataki Visitor Centre, Auckland, New Zealand	*Agathis australis*	Unpublished data
Craig Barton	Glencorse near Edinburgh Scotland	*Picea sitchensis*	Barton & Jarvis (1999) New Phytologist.
David Ellsworth	Duke Forest, Durham, NC, USA	*Pinus taeda*	Ellsworth DS (1999) Plant, Cell & Environment.
David Ellsworth	Richmond, Sydney, Australia	*Eucalyptus saligna*	Unpublished data
David Ellsworth	Richmond, Sydney, Australia	Four *Eucalyptus* species	Héroult et al. (2013) Plant, Cell & Environment.
David Tissue	Big Bend National Park, Texas, USA	*Larrea tridentata*	Ogle et al. (2012)
Derek Eamus	Palmerston, NT, Australia	A set of six savanna tree species	Thomas & Eamus (2002) Australian Journal of Botany.
Derek Eamus	Western Sydney, Castlereagh, Australia	*Angophora bakeri* & *Eucalyptus parramattensis*	Zeppel et al. (2008) Australian journal of botany.
Harvard forest data archive	Prospect Hill Tract, Harvard Forest, USA	A set of four deciduous angiosperm tree species	Bassow & Bazzaz (1997) Oecologia.
Jean-Marc Limousin	Sevilleta NWR, PJ rainfall manipulation, USA	*Juniperus monosperma* & *Pinus edulis*	Limousin et al. (2013) Plant, Cell & Environment.
Jeff Kelly	Daintree forest, Cape Tribulation, QLD, Australia	A set of three tropical rainforest species	Unpublished data
Jeff Warren	ORNL FACE, TN, USA	*Liqiudambar styraciflua*	Warren et al. (2011) Ecohydrology.
Jesse Nippert	Konza Prairie, KS, USA	A set of C3 and C4 grassland species	Unpublished data
Joana Zaragoza-Castells, Patrick Meir & Owen Atkin	French Guiana	A set of tropical rainforest species	Unpublished data

Joana Zaragoza-Castells, Patrick Meir & Owen Atkin	Tambopata, Peru	A set of tropical species	Unpublished data
Johan Uddling	Rhinelander, WI, USA	*Betula papyrifera* & *Populus tremuloides*	Uddling et al (2009) Tree Physiology
John Drake	Duke Forest, Durham, NC, USA	*Pinus taeda*	Drake et al. (2011) Global Change Biology
Jonathan Bennie	Agoufou, Hombori, Mali	A set of African savanna tree species	Unpublished data
David Tissue	Narrabri, NSW, Australia	Cotton	Unpublished data
Kohei Koyama & Kihachiro Kikuzawa	Ishikawa, Japan	*Fagus crenata*	Koyama and Kikuzawa 2012 Ecological Research.
Kouki Hikosaka	Aobayama, Sendai, Japan	A set of nine angiosperm and gymnosperm tree species	Hikosaka and Shigeno (2009) Oecologia.
Kouki Hikosaka	TOEF, Tomakomai, Hokkaido, Japan	*Quercus crispula*	Hikosaka et al (2007) Tree Physiology.
Lasse Tarvainen & Göran Wallin	Skogaryd, Sweden	*Picea abies*	Tarvainen et al. (2013) Oecologia.
Lindsay Hutley & Samantha Setterfield	Wildman River, NT, Australia	*Alloteropsis semialata* & *Andropogon gayanus*	Unpublished data
Lisa Wingate	Aberfeldy, UK	*Picea sitchensis*	Wingate et al. (2007) Plant, Cell & Environment.
Lucas Cernusak	Howard Springs, NT, Australia	A set of evergreen savanna tree species	Cernusak et al. (2011) Agriculture & Forest Meteorology.
Lucas Cernusak	Daly River, NT, Australia	A set of evergreen savanna tree species	Cernusak et al. (2011) Agriculture & Forest Meteorology.
Lucas Cernusak	Dry River, NT, Australia	A set of evergreen savanna tree species	Cernusak et al. (2011) Agriculture & Forest Meteorology.
Lucas Cernusak	Adelaide River, NT, Australia	A set of evergreen savanna tree species	Cernusak et al. (2011) Agriculture & Forest Meteorology.
Lucas Cernusak	Sturt Plains, NT, Australia	A set of evergreen savanna tree species	Cernusak et al. (2011) Agriculture & Forest Meteorology.
Lucas Cernusak	Boulia, QLD, Australia	A set of evergreen savanna tree species	Cernusak et al. (2011) Agriculture & Forest Meteorology.
Lucy Rowland & Patrick Meir	Caxiuana, Brazil	*Manilkara spp.*	Unpublished data
Maj-Lena Linderson & Teis Nørgaard Mikkelsen	Soroe, Denmark	*Fagus sylvatica*	Linderson et al. (2012) Agriculture & Forest Meteorology

Mark Broadmeadow	Headley S. London, UK	Three Quercus species	Broadmeadow et al. (1999) Water, Air and Soil Pollution.
Markus Löw	Kranzberg forest, Germany	*Fagus sylvatica*	Op de Beeck et al. (2010) Agriculture & Forest Meteorology.
Michael Freeman	Soroe, Denmark	*Fagus sylvatica*	Freeman, M. (1998) PhD Thesis.
Nicolas Martin-StPaul	Les Mages, France	*Quercus ilex*	Martin-StPaul et al. (2012) Functional Plant Biology.
Nicolas Martin-StPaul	Puechabon, France	*Quercus ilex*	Martin-StPaul et al. (2012) Functional Plant Biology.
Nicolas Martin-StPaul	Vic la Gardiole, France	*Quercus ilex*	Martin-StPaul et al. (2012) Functional Plant Biology.
Oula Ghannoum	Brian Pastures Res. Stn, Gayndah, QLD, Australia	A set of C4 grasses	Unpublished data
Paolo de Angelis	Montalto di Castro, Italy	*Phillyrea angustifolia*, *Pistacia lentiscus* & *Quercus ilex*	Scarascia-Mugnozza et al. (1996) Plant, Cell & Environment.
Pasi Kolari	Hyytiälä, Finland	*Pinus sylvestris*	Kolari et al. (2007) Tellus.
Patrick Mitchell	Corrigin Water Reserve, WA, Australia	*Eucalyptus capillosa* & *Eucalyptus salmonophloiia*	Mitchell et al. (2009) Agriculture & Forest Meteorology.
Qingmin Han	FFPRI, Tsukuba, Ibaraki, Japan	*Chamaecyparis obtusa*	Han et al. (2009) Journal of forest research.
Qingmin Han	Mt Fuji, Japan	*Pinus densiflora*	Han et al. (2003) Tree Physiology.
Maarten Op de Beeck	Tervuren, Belgium	*Brassica napus* & *Brassica oleracea*	Op de Beeck et al. (2010) Environmental Pollution.
Sabine Tausz-Posch	AGFACE facility, Horsham, VIC, Australia	*Triticum aestivum* two varieties	Tausz-Posch et al. (2013) Physiologia Plantarum.
Teresa E. Gimeno	Alto Tajo Natural Park, Guadalajara, Spain	*Juniperus thurifera*	Gimeno et al. (2012) Tree Physiology.
Victor Resco de Dios	Santa Rita Experimental Range, USA	*Eragrostis lehmanniana* & *Heteropogon contortus*	VRD et al. (2012) Prespectives in Plant Ecology, Evolution and Systematics.
Wei Sun	Charleston mesquite site, Tombstone, AZ, USA	A set of mesquite C3 and C4 grass species	Sun et al. (2009) Plant, Cell & Environment.
Wei Sun	San Pedro, Sierra Vista, AZ, USA	A set of riparian C3 and C4 grass species	Sun et al. (2010) Oecologia.
Yusuke Onoda	Hakkoda, Aomori, Japan	*Fagus crenata*, *Lindera umbellata* & *Magnolia salicifolia*	Yasumura et al. (2005) & Onoda unpublished.

433 **Table S2: Estimates of g_1 by different classification schemes.**

Classification scheme	Class	g_1 mean	g_1 SE	Number of data points	Number of species
a_Pathway	C4	1.62	0.03	1161	38
	C3	4.16	0.01	14001	276
b_Plantform	Gymno. tree	2.35	0.02	4732	13
	shrub	3.32	0.05	689	15
	Angio. tree	3.97	0.02	6265	203
	Grass	5.25	0.13	304	20
	Savanna tree	5.76	0.22	339	20
	Crop	5.79	0.04	1672	5
c_T region	Arctic	2.22	0.07	162	8
	Boreal	2.19	0.02	917	5
	Temperate	4.31	0.02	11934	75
	Tropical	4.43	0.08	988	189
d_W region	MI < 0.5	3.77	0.03	3328	17
	0.5<MI<1.0	4.69	0.04	1673	45
	1.0<MI<1.5	3.87	0.03	4313	29
	MI<1.5	4.02	0.02	4687	186
e_PFTs	C4 grass	1.62	0.03	1161	38
	Ever. gymno. tree	2.35	0.02	4732	13
	Deci. savanna tree	2.98	0.39	30	2
	Shrub	3.32	0.05	689	15
	Ever. angio. tree	3.37	0.03	2828	17
	Trop. Rainforest tree	3.77	0.06	549	167
	Deci. angio. tree	4.64	0.04	2888	19
	C3 grass	5.25	0.13	304	20
	C3 crop	5.79	0.04	1672	5
	Ever. savanna tree	7.18	0.25	309	18

434

Table S3: Model coefficients for g_1 as a function of MI and $mGDD_0$. The model was fitted with a linear mixed-effects model as $\log(g_1) \sim MI+mGDD_0+MI*mGDD_0$ using different PFTs as the random effects to account for the differences in intercept among PFTs.

	Model		
Variables	**mean**	**SE**	**DF**
Intercept	0.449	0.289	97
MI	0.033	0.013	97
$mGDD_0$	0.027	0.192	97
MI*$mGDD_0$	0.014	0.012	97

Supplementary Figure legends

Fig. S1: Climatic space covered by the Stomatal Behaviour Synthesis Database. Shown as a combination of mean annual temperature (MAT; ^{o}C), mean annual precipitation (MAP; mm), mean annual degree days above 0^{o}C (mGDD$_{0;}$ ^{o}C) and moisure index (MI).

Fig. S2. Residual plot by PFTs for the model: log(g_1)~ MI+mGDD$_0$+MI*mGDD$_0$. The model was fitted using linear mix-effects model with PFTs as the random effect to account for the differences in intercept among PFTs.

Fig. S3. predicted log(g_1) as a function of mGDD$_0$ and MI. (a) the predicted log(g_1) under different ranges of MI and mGDD$_0$ presented as partial regression plot. Predictions are from linear mixed-effects model for log(g_1) assuming PFTs as a random effect to account for the differences in intercept among PFTs. Colour lines represent the predicted g_1 based on fitted model coefficients (Table S3). Colour dots represent the partial regression predictions at a given fixed MI or mGDD$_0$ level.

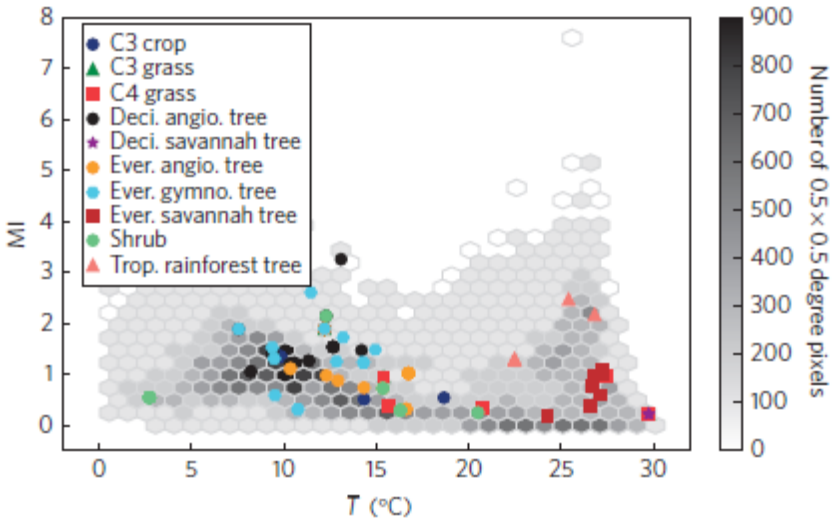

Figure 1 | Climatic space covered by the Stomatal Behaviour Synthesis Database, shown as mean temperature during the period with daily mean temperatures above 0 °C and moisture index. Coloured circles represent climatic space for the database, with different colours indicating different plant functional types. Grey hexagons represent global climatic space for which vegetation is present. The global climatic space data were binned by every 1 °C for temperatures above 0 °C ($\bar{T}$) and every 0.25 for the moisture index (MI). The grey scale bar indicates the number of 0.5 × 0.5 degree pixels for a given binned $\bar{T}$ and MI combination.

461

462

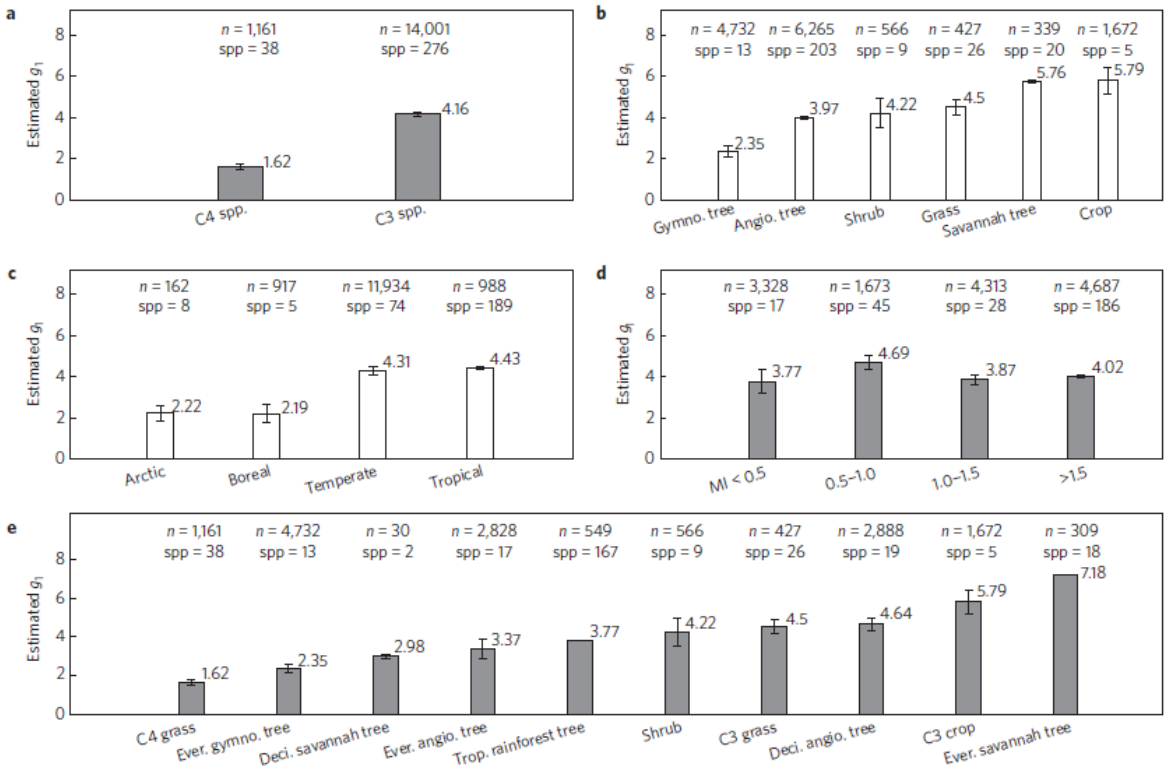

Figure 2 | Mean g_1 values for plant functional types defined by different classification schemes. Each bar represents the mean values ± 1SE of g_1 from the stomatal model fitted using a nonlinear mixed-effects model assuming species as a random effect. The sample sizes (n) are the number of measurements. In the case of diurnal measurements, measurements might be done on the same leaf but under different environmental conditions. Species number (spp) indicates the number of the species in each group. Panels **b–d** include C_3 species data only.

463

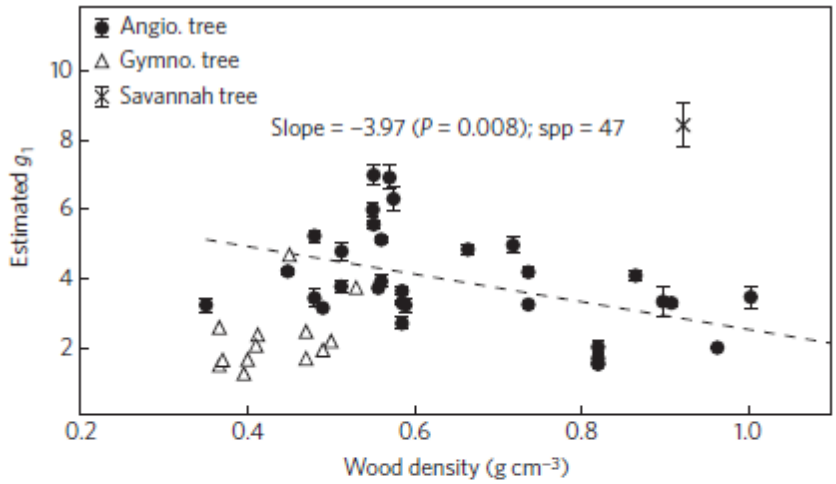

Figure 3 | Relationship between g_1 and wood density for angiosperm and gymnosperm trees. Savannah tree species (all of which were angiosperms) are indicated separately. Each data point represents mean ± 1SE of g_1 for an individual species fitted with a nonlinear regression model. A linear regression line was fitted only for angiosperm trees due to the lack of a significant linear relationship for gymnosperm trees. The fitted linear regression relationship between g_1 and wood density for angiosperm trees is: $g_1 = -3.97^{*}WD + 6.53$ ($P = 0.0008$, $R^2 = 0.21$). Wood density data were obtained from Global Wood Density Database[2,29] and are available for 47 species in the Stomatal Behaviour Synthesis Database. The wood density database is a collection of published data based on actual measurements.

464

465

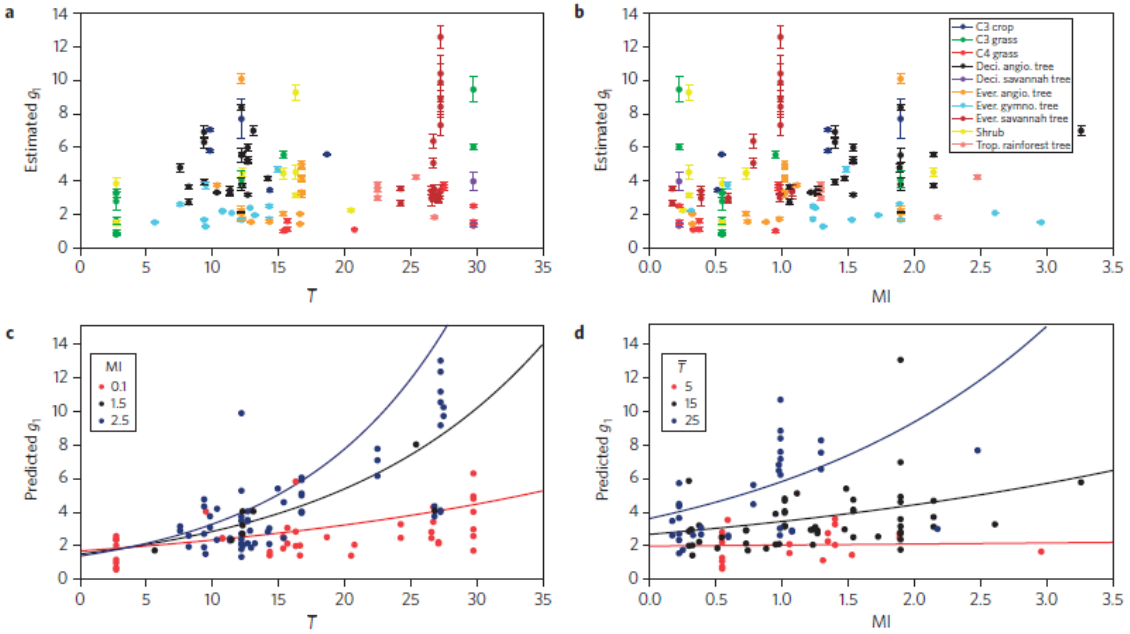

Figure 4 | Estimated and predicted g_1 as a function of $\bar{T}$ and MI. a,**b**, Relationship between estimated g_1 and mean temperature during the period with daily mean temperatures above 0 °C ($\bar{T}$; °C) (**a**) and moisture index (MI) (**b**) at experimental sites among species across different plant functional types (PFTs). Each data point represents the mean ± 1SE of g_1 for individual species fitted with a nonlinear regression model. Classification of plant functional types are shown in Fig. 2e. **c**,**d**, Predicted g_1 under different ranges of MI (**c**) and $\bar{T}$ (**d**) presented as a partial regression plot. Predictions in **c** and **d** are from a weighted linear mixed-effects model for $\log(g_1)$ using the inverse of the SE of g_1 as weights to account for the uncertainty of g_1 fitting and assuming PFTs as a random effect to account for the differences in intercept among PFTs. Coloured lines represent the predicted g_1 based on fitted model coefficients (Supplementary Table 5). Coloured dots represent the partial regression predictions at a given fixed MI or $\bar{T}$ level.

466